Surface reconstruction and relaxation of Al(110)-$c(2\times2)$-Na

A. Mikkelsen
Institute of Physics and Astronomy, Aarhus University, DK-8000 Aarhus C, Denmark

S. V. Hoffmann
Institute of Storage Ring Facilities, Aarhus University, DK-8000 Aarhus C, Denmark

J. Jiruse
Department of Physical Engineering, Institute of Mechanical, Engineering, Technicka 2, 616 69 Brno, Czech Republic

D. L. Adams
Institute of Physics and Astronomy, Aarhus University, DK-8000 Aarhus C, Denmark
(Received 27 October 1999)

The surface structure of the Al(110)-$c(2\times2)$-Na phase, formed by adsorption of 0.5 ML Na on Al(110) at room temperature, is shown by analysis of extensive low-energy electron diffraction measurements to contain Na atoms in twofold substitutional sites formed by displacement of 0.5 ML Al atoms from the first layer of the substrate. The reconstructive adsorption leads to strong perturbations of the substrate extending to the fifth Al layer. A large rumpling (0.15 Å) of the third Al layer is found, together with a smaller rumpling (0.06 Å) of the fifth layer. Al atoms in the third Al layer, which are directly below Na atoms, exhibit enhanced vibrations as compared to the remaining atoms of the layer.

I. INTRODUCTION

The adsorption of alkali metals on Al(110) is of particular interest in that extrapolation of the results of previous studies of alkali metal adsorption on Al surfaces, and previous studies of alkali metal adsorption on fcc(110) metal surfaces, lead to quite different expectations of the adsorption behavior on Al(110). Thus, on the one hand, recent studies of alkali metal adsorption[1–5] on Al(111) and (100) at room temperature have shown that the adsorption leads to a reconstruction of the substrate, with alkali atoms located in substitutional sites. On the other hand, small ($\sim$0.1 ML) coverages of alkali metals on Ni, Cu, Ag, and Pd(110) induce (1×2), ''missing-row'' reconstructions,[6–8] similar to the intrinsic (1×2), missing-row reconstructions[9–12] of clean Pt, Ir, and Au(110). It has been suggested[13,14] that the adsorption of alkali metals on fcc(110) metal surfaces is in general likely to induce missing-row structures, because of the small energy difference between the (1×1) and (1×2) structures for the clean surfaces, and because of the larger binding energy of the alkali atoms in sites of high coordination in the missing rows. The latter suggestion has been confirmed in the case of Cu(110)/K by a photoelectron diffraction study.[15]

In work described elsewhere,[16,17] core-level photoemission and qualitative low-energy electron diffraction (LEED) measurements of the adsorption of Li, Na, K, Rb, and Cs on Al(110) indicate that Al(110) does not follow the pattern of other fcc(110) metals in forming (1×2) missing-row structures. However, the adsorption behavior also differs in many respects from that found for Al(111) and (100). Adsorption of Na on Al(110) leads to the formation of $c(2\times2)$, (3×1), and (4×1) phases with increasing coverage. Adsorption of K, Rb, and Cs leads to the formation of $c(4\times2)$ and $c(2\times2)$ phases with increasing coverage, although neither phase is well ordered in the case of K, and only the $c(4\times2)$ phases are well ordered in the case of Rb and Cs. Adsorption of Li leads to a single, well-ordered, $c(2\times2)$ phase.

In this study we describe the results of a *quantitative* structure determination for an alkali metal adsorbed on Al(110), namely, for the $c(2\times2)$-Na phase formed by adsorption of 0.5 ML Na. For this phase, the adsorption follows the pattern of adsorption on Al(111) and (100) to the extent that Na is found to adsorb in substitutional sites, with displacement of 0.5 ML Al atoms from the first layer of the substrate. The reconstructive adsorption causes strong perturbations of the surface relaxations and vibrations of the clean Al(110) surface.

In the following, the experimental procedures used here are described in Sec. II. The procedures used in calculating LEED intensities, and the use of the intensities in analyzing the experimental data, are described in Sec. III. The results of the analysis are presented in Sec. IV and discussed in Sec. V.

II. EXPERIMENT

The measurements were carried out in a new Vacuum Generators μ-metal ultrahigh vacuum chamber with base pressure of $\leqslant1\times10^{-10}$ torr. LEED intensity measurements were carried out using an Omicron reverse-view LEED optics and a newly developed digital-LEED system in which the LEED pattern on the fluorescent screen of the reverse-view LEED optics is recorded using a 16-bit Princeton slow-scan, Peltier-cooled, charge-coupled device (CCD) camera with Nikkor 28 mm $f/2.0$ lens. The digital images are stored on disk and analyzed off line to obtain the intensities of the

diffracted beams, as described elsewhere.[18] Auger electron spectrocopy (AES) measurements of surface chemical composition were made using a Vacuum Generators AX100 electron spectrometer. The Al(110) crystal could be cooled to 100 K using liquid nitrogen and heated by electron bombardment. The crystal was cleaned by cycles of Ar^+ bombardment and annealing to 670 K. It should be noted that the annealing temperature used for the Al(110) face is 50 K lower than used on the more close-packed Al faces. This resulted in a more well-ordered surface, as judged by the quality of the LEED patterns, than obtained in our earlier studies of this surface.[19] Sodium was deposited onto the crystal by evaporation from a thoroughly degassed SAES source.[20] The deposition was carried out in a few minutes and the residual-gas pressure during evaporation rose less than 5×10^{-11} torr. AES measurements taken after deposition and after completion of a set of LEED measurements indicated that surface contamination of S, C, and O was always less than 0.03 ML.

Adsorption of Na on Al(110) at room temperature leads to the formation of a $c(2\times2)$ LEED pattern with split fractional-order spots at a coverage of about 0.4 ML. A sharp $c(2\times2)$ LEED pattern with good contrast is obtained after deposition of 0.5 ML Na. As noted above, (3×1) and (4×1) phases are formed at higher Na coverages.[16,17] An optimally developed $c(2\times2)$ structure can also be obtained by adsorption of >0.8 ML followed by anealing to 410 K. Desorption of Na occurs at temperatures greater than 475 K with restoration of the original (1×1) LEED pattern. The method of annealing was used to prepare the $c(2\times2)$ phase for which LEED intensity-energy spectra were measured in this study.

Intensity-energy spectra were measured for the $c(2\times2)$-Na phase at 100 K, in the energy range 40–440 eV with a step size of 1 eV, at normal incidence $\gamma,\phi,\theta=0°$, and at off-normal incidence $\gamma,\phi=0°$, $\theta=10°$, where γ and θ are rotational angles about perpendicular axes lying in the plane of the crystal, and ϕ is the azimuthal angle, consisting of a rotation about the surface normal. The condition $\phi=0°$ was chosen to preserve mirror-plane symmetry for measurements at $\theta=10°$. Normal incidence was set to within $\theta=\pm0.1°$ and $\gamma=\pm0.1°$ by minimizing the R factor defined below for the comparison of intensity-energy spectra for symmetry-equivalent beams as a function of these two angles. The precision of the geometry at off-normal incidence, which involved setting $\phi=0°$ by aligning the [001] direction in the LEED pattern with the horizontal, is less certain due to possible errors in the mutual alignment of the crystal goniometer and the LEED optics. However, subsequent comparisons of experimental and *calculated* intensity-energy spectra as a function of θ indicated that the precision of the incidence geometry was also of the order of $\pm0.1°$ for $\theta=10°$. As in previous studies using our old video-LEED system,[21] it was found that the discrepancies between spectra for symmetry-equivalent beams were larger than the very small random errors between repetitive measurements for the same beam. The spectra shown later are the result of averaging the intensities of symmetry-equivalent beams of just one set of measurements, which is sufficient to obtain very high quality spectra due to the 16-bit dynamic range and low noise of the CCD camera. Intensity-energy spectra were recorded for all excited beams having a energy range greater than about 30 eV, except for a few beams whose trajectories intersected the shadow on the fluorescent screen of the connections to the electron gun. This led to a total of 25 symmetry-inequivalent beams at $\theta=0°$ (15 integral order and 10 fractional order) and 32 symmetry-inequivalent beams at $\theta=10°$ (18 integral order and 14 fractional order).

III. LEED INTENSITY CALCULATIONS AND STRUCTURAL ANALYSIS

LEED intensities were calculated using the dynamical theory of LEED, with computer programs[22,23] derived from the layer-doubling and combined-space programs of Pendry[24] and of Van Hove and Tong.[25] Atomic scattering matrices for Al and Na were calculated using phase shifts calculated from the muffin-tin band-structure potentials of Moruzzi *et al.*,[26] and were renormalized for the effects of thermal vibrations using rms isotropic vibrational amplitudes u_j for atoms in the jth layer. The vibrational amplitudes are defined here by the time-average displacement given by $u^2=u_1^2+u_2^2+u_3^2$ ($=3u_1^2$ for isotropic vibrations) where $u_{1,2,3}$ are the time-average values of the projection of **u** on three orthogonal axes.[27] The complex electron self-energy $\Sigma=V_0+iV_{im}$ was taken to be independent of energy. At the highest energy, 324 partial waves (18 phase shifts, $l_{\max}=17$) and 321 plane waves (reduced by symmetry to 88 and 171 symmetry-adapted plane waves at $\theta=0°$ and $\theta=10$, respectively) were used in the L-space and k-space treatments, respectively, of multiple scattering within and between layers parallel to the surface. The surface potential barrier was taken to be a refracting but nonreflecting step of height V_0, positioned at a distance equal to one-half the bulk interlayer spacing above the first layer of atoms. The calculations are a numerically accurate[28] reflection of the model assumptions to about 0.2 %. All calculations used in the structure determination were carried out with full accuracy.

Refinement of the surface structure of Al(110)-$c(2\times2)$-Na was carried out using a semiautomatic implementation of an iterative procedure described previously,[23] in which the disagreement between experimental and calculated intensities, as measured by an R factor, is minimized as a function of one variable at a time. The procedure contains an inner loop in which the structural variables are optimized iteratively, and an outer loop in which the nonstructural variables are optimized iteratively. The inner loop is executed automatically in a single computer run, but the outer loop is currently executed manually. The procedure is very efficient by virtue of maximum reuse of intermediate calculations. The R factor used here is a normalized χ^2 function defined[4,29,30] as

$$R=1-\left[\sum_{hk,i}\left(\frac{I^{ex}_{hk,i}I^{cal}_{hk,i}}{\sigma_{hk}}\right)\right]^2\Bigg/\sum_{hk,i}\left(\frac{I^{ex}_{hk,i}}{\sigma_{hk}}\right)^2\sum_{hk,i}\left(\frac{I^{cal}_{hk,i}}{\sigma_{hk}}\right)^2 \tag{1}$$

in terms of the experimental $I^{ex}_{hk,i}$ and calculated intensities $I^{cal}_{hk,i}$, where the index i runs over the electron energy, and σ_{hk}, the root-mean-square experimental uncertainty of the beam hk, obtained[4] via comparison of measurements for symmetry-equivalent beams. Implicit in this definition of R

is the use of a *single* scaling constant between the experimental and calculated intensities.

IV. RESULTS

In the initial stage of the structure determination, a preliminary survey was carried out of structural models involving Na atoms adsorbed in on-top, twofold hollow, twofold short and long-bridge, and twofold substitutional sites, compatible with the symmetry of the measured LEED intensities. Although no optimization of the nonstructural parameters was carried out in this survey, the results indicated unequivocally that only the twofold substitutional site warranted further refinement. The possibility that the 0.5 ML of Al atoms displaced by Na atoms are readsorbed in high-symmetry sites was also investigated, but found to be incompatible with the measured intensities. We assume, therefore, that the displaced Al atoms are readsorbed at surface steps. The R factors for the discarded models were in the range 0.25–0.35 as compared to the value of 0.045 found for the optimal model in the analysis of the normal-incidence data, as described below.

A full optimization of the fit between experimental intensities and intensities calculated for Na adsorbed in the twofold substitutional site was carried out using the procedure described above. The structural variables consisted of the first seven interlayer spacings d_{ij} and a rumpling Δr_3 and Δr_5 of the third and the fifth Al layers. The spacing between the $c(2\times2)$-Na layer and the $c(2\times2)$-Al layer is denoted d_{01}. For each of the two rumpled layers, the sense of the rumpling is that Al atoms lying on the rotation axis through adsorbed Na atoms move towards the surface and Al atoms in the second $c(2\times2)$ sublattice move towards the bulk, as shown in Fig. 1(b). The interlayer spacings d_{23}, d_{34}, d_{45}, and d_{56}, involving the two rumpled layers, are defined with respect to the positions of the two sublattices of each rumpled layer, rather than with respect to the midpoints of the layers. The nonstructural variables were the rms vibrational amplitudes u_0 of adsorbed Na atoms, u_i of Al atoms in the first five Al layers, and u_{bulk} of Al atoms in the bulk, together with V_0 and V_{im}. Separate vibrational amplitudes u_{3a} and u_{3b} were assigned to Al atoms in the two sublattices of the third, rumpled Al layer, where u_{3a} are the amplitudes for Al atoms directly beneath Na atoms.

The results of the independent refinements for measurements at $\theta=0°$ and $\theta=10°$ are listed in Table I, together with the results of our recent LEED analysis[31] for the clean Al(110) surface. As can be seen from the table, good agreement exists between the results of the analyses for $\theta=0°$ and $\theta=10°$. A model of the substitutional $c(2\times2)$-Na structure, constructed using the average values of the structural parameters from the two independent analyses, is shown in Fig. 1. The main feature of the structure is that Na atoms occupy substitutional sites in a reconstructed Al layer. The Na-Al interlayer spacing is 1.06 Å, corresponding to a hard-sphere radius of 1.62 Å for the adsorbed Na atoms, as compared to the bulk bcc radius of 1.86 Å. A second notable feature of the structure is the large rumpling of the third and fifth Al layers of 0.14 Å and 0.06 Å, respectively.

Plots of some of the experimental intensity-energy spectra and spectra calculated for the optimum parameter values given in Table I are shown in Figs. 2 and 3. We note that the plots have been constructed using a single, beam-independent, scaling factor between the experimental and calculated spectra. Thus the good agreement between experiment and theory also includes agreement between the relative intensities of the different beams.

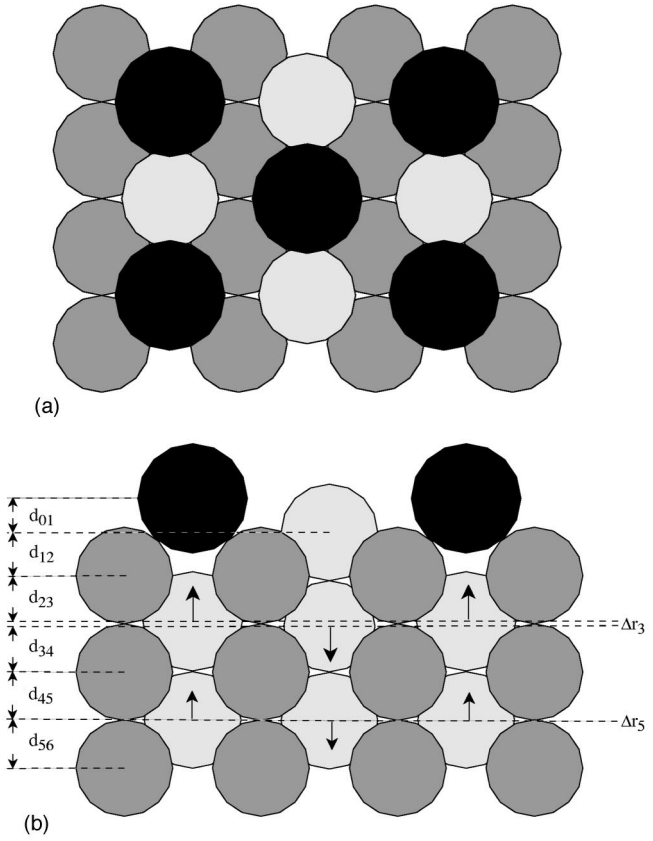

FIG. 1. Hard-sphere model of the geometry of the Al(110)-$c(2\times2)$-Na structure. (a) Top view, shown as a projection on the (110) plane; (b) side view, shown as a projection on the $(1\bar{1}0)$ plane. The shading indicates atoms lying in the same planes perpendicular to the plane of the drawings. Black circles indicate the position of Na atoms. Arrows in (b) indicate the sense of the rumpling of the third and fifth Al layers. See text.

V. DISCUSSION

A. Substitutional adsorption

The results presented here show that the stable binding geometry for 0.5 ML Na adsorbed on Al(110) involves Na atoms adsorbed in substitutional sites formed by displacement of 0.5 ML Al atoms from the first layer of the substrate. Thus at first glance, the adsorption of Na on Al(110) appears to fit the pattern of previous results for the adsorption of alkali metals on Al, rather than the pattern of formation of (1×2) missing-row structures as found for adsorption of low coverages of alkali metals on other fcc(110) metal surfaces. However, LEED pattern and core-level measurements[16,17] indicate that the substitutional structure is formed in a rather narrow coverage window around 0.5 ML, which differs from the adsorption behavior for Al(111) and Al(100), where island formation of substitutional structures is the rule at lower coverages.

TABLE I. Best-fit parameter values for Na adsorbed in the twofold substitutional site in the Al(110)-$c(2\times2)$-Na structure. The interlayer spacings are denoted d_{ij} and the rms vibrational amplitudes are denoted u_j, where the subscripts indicate the layers in question. See text.

Phase incidence angle	Clean Al(110) $\theta=0°$	Al(110)-$c(2\times2)$-Na $\theta=0°$	$\theta=10°$	Average
d_{01}		1.06±0.03 Å	1.05±0.03 Å	1.06±0.02 Å
d_{12}	1.31±0.03 Å	1.28±0.02 Å	1.25±0.02 Å	1.27±0.01 Å
d_{23}	1.51±0.03 Å	1.35±0.03 Å	1.37±0.03 Å	1.36±0.02 Å
d_{34}	1.37±0.03 Å	1.36±0.03 Å	1.35±0.03 Å	1.36±0.02 Å
d_{45}	1.44±0.02 Å	1.38±0.03 Å	1.38±0.03 Å	1.38±0.02 Å
d_{56}		1.40±0.03 Å	1.40±0.05 Å	1.40±0.03 Å
d_{67}		1.42±0.04 Å	1.41±0.06 Å	1.42±0.03 Å
Δr_3		0.15±0.03 Å	0.14±0.02 Å	0.14±0.02 Å
Δr_5		0.06±0.04 Å	0.05±0.05 Å	0.06±0.03 Å
u_0		0.27±0.04 Å	0.27±0.03 Å	0.27±0.02 Å
u_1	0.17±0.04 Å	0.17±0.04 Å	0.17±0.03 Å	0.17±0.02 Å
u_2	0.17±0.08 Å	0.13±0.04 Å	0.13±0.03 Å	0.13±0.02 Å
u_{3A}	0.13±0.04 Å	0.17±0.04 Å	0.14±0.04 Å	0.16±0.03 Å
u_{3B}	0.13±0.04 Å	0.11±0.04 Å	0.09±0.04 Å	0.10±0.03 Å
u_4		0.10±0.04 Å	0.10±0.04 Å	0.10±0.03 Å
u_5		0.11±0.04 Å	0.10±0.04 Å	0.10±0.03 Å
u_{bulk}	0.06±0.02 Å	0.10±0.04 Å	0.15±0.10 Å	0.11±0.04 Å
V_{im}	5.1±0.7 eV	4.1±0.6 eV	3.2±0.5 eV	3.7±0.4 eV
$R_{\text{exp-theory}}$	0.039	0.045	0.042	

In discussing possible reasons for the formation of the substitutional $c(2\times2)$-Na structure, rather than a missing-row structure, it can be noted that the former process can be thought of as occuring in two steps, in which an Al atom is removed from the surface and rebonded at a surface step, followed by adsorption of a Na atom in the vacancy. Similarly, the latter process can be thought of as a reconstruction of the (1×1) surface to a (1×2) missing-row structure, followed by adsorption of Na atoms in sites in the troughs of the missing rows. *Ab initio*[32] calculations of vacancy formation, and effective-medium calculations[14] of the reconstruction energy of the Al(110) surface, indicate that these energies are roughly equal with a value of ~0.12 eV. This suggests that the energy required for reconstruction of the substrate is not the deciding factor in the choice of adsorption site. We presume therefore that the adsorption energy in the substitutional site is larger than the adsorption energy in sites in the troughs of the missing-row structure. In this regard it is interesting to note that the Al(110)-$c(2\times2)$-Na structure determined here is almost identical to the Au(110)-$c(2\times2)$-K structure proposed by Ho *et al.*[33] on the basis of *ab initio* calculations, and later confirmed by an ion-scattering study.[34] Ho *et al.* suggested that K atoms adsorb in the troughs of the intrinsic missing-row structure at low coverage, but form a structure of the kind shown in Fig. 1 at higher coverage, in order to minimize the large electrostatic energy associated with K ions sitting in adjacent sites in the missing rows. Ho *et al.* noted further that the fact that Au forms bulk alloys with Na suggests that formation of a surface alloy might be energetically feasible. In the light of the present results it is interesting to speculate that the substitutional $c(2\times2)$ structure, as formed on Au and Al(110), might in fact be the configuration of lowest energy for the fcc(110) metals that form missing-row structures on adsorption of alkali metals, but that its formation is hindered by an activation energy barrier, which can be overcome at room temperature on Al and Au. In detail, of course, the mechanisms of formations of the Al(110)-$c(2\times2)$-Na and Au(110)-$c(2\times2)$-K structures must be different, in that the formation of the former requires displacement and readsorption of 0.5 ML Al atoms, whereas formation of the latter structure requires only a place exchange of Au and K atoms.

B. Substrate reconstruction and relaxation induced by superstructure formation

As can be seen from the results in Table I, the primary reconstruction of the substrate due to the substitutional adsorption of Na is accompanied by a secondary reconstruction involving a rumpling of the third and fifth Al layers. A considerable modification of the interlayer relaxations of the clean Al(110) surface also occurs. The layer rumplings and interlayer relaxations found for Al(110)-$c(2\times2)$-Na and Au(110)-$c(2\times2)$-K are listed together with the interlayer relaxations[31] of clean Al(110) in Table II. As can be seen from the table, the strong similarity between the Al(110)-$c(2\times2)$-Na and Au(110)-$c(2\times2)$-K structures also extends to the reconstruction and relaxation of the substrate. It can also be seen from the table that the oscillatory nature of the multilayer relaxations for the clean Al(110) surface is replaced by a contraction of all intralayer spacings.

As discussed elsewhere,[35,36] the occurence of substrate reconstruction is an expected consequence of the loss of translational symmetry due to the formation of a superstructure. For a number of systems, including Al(110)-$c(2\times2)$-Na, we have shown recently[35] that the trends of the

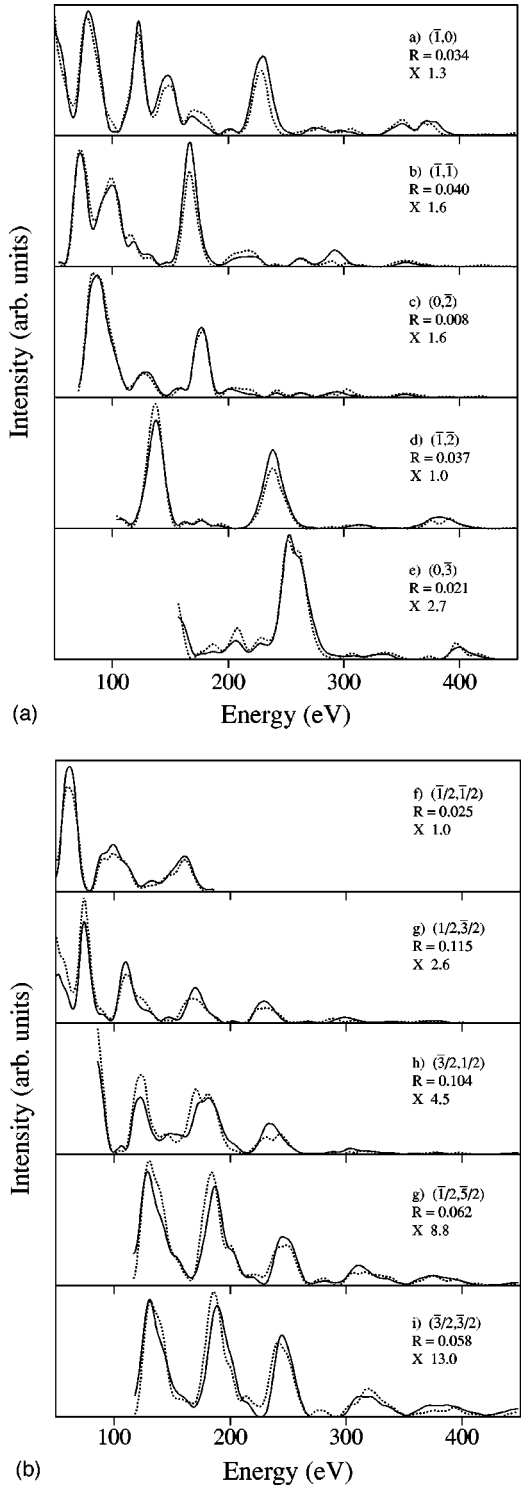

FIG. 2. Comparison of experimental (solid lines) and calculated (dotted lines) intensity-energy spectra for Al(110)-$c(2\times2)$-Na at $\theta=0°$ for five integral-order beams (a)–(e), and five fractional order beams, (f)–(j). The beam hk indices, R factors, and scale factors are shown in each panel. The calculated spectra were obtained using the best-fit parameter values given in Table I.

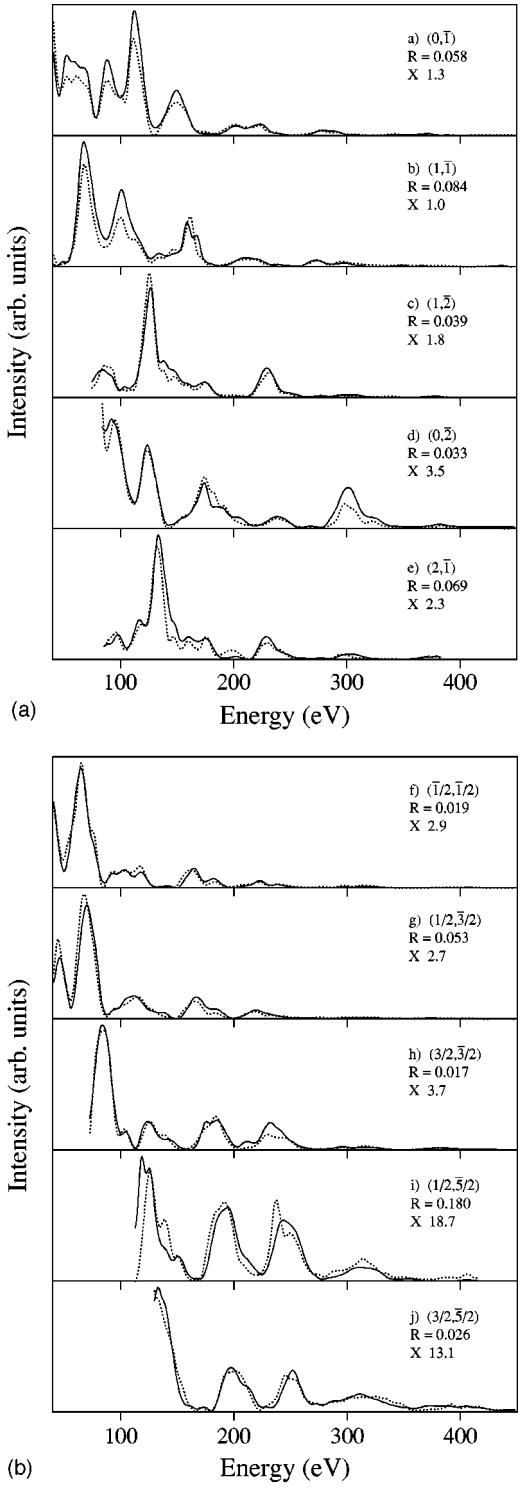

FIG. 3. Comparison of experimental (solid lines) and calculated (dotted lines) intensity-energy spectra for Al(110)-$c(2\times2)$-Na at $\theta=10°$ for five integral-order beams (a)–(e), and five fractional order beams, (f)–(j). The beam hk indices, R factors, and scale factors are shown in each panel. The calculated spectra were obtained using the best-fit parameter values given in Table I.

reconstructive layer displacements and the interlayer relaxations can be predicted by consideration of the electrostatic forces on the layers of the *unrelaxed* substrate in a simple point-ion/frozen background (PIFB) model.[23,35] The predictions of the model for clean Al(110), Al(110)-$c(2\times2)$-Na, and Au(110)-$c(2\times2)$-K are also listed in Table II. In the PIFB calculations, charges of 1 were used for Na, K, and Au, and a charge of 3 was used for Al. In the calculations for the $c(2\times2)$ structures, the adsorbed layers were placed at the experimentally-determined positions with respect to the first,

TABLE II. Comparison of experimental [LEED and medium-energy ion scattering (MEIS)] and calculated (DFT and PIFB) substrate reconstruction and intralayer relaxation for clean Al(110), Al(110)-$c(2\times2)$-Na, and Au(110)-$c(2\times2)$-K. Relaxations $\Delta d_{12}, \Delta d_{23}, \Delta d_{34}$, and Δd_{45} of the first four interlayer spacings are expressed as percent deviations from the corresponding bulk values. The interlayer spacings involving rumpled layers are defined by taking the nearest distance between the two layers. The vertical separations between the two sublattices of the rumpled third and fifth bulk layers Δr_3 and Δr_5 are also expressed as percentages of the bulk interlayer spacing.

Phase	Al(110)-(1×1)		Al(110)-$c(2\times2)$-Na		Au(110)-$c(2\times2)$-K		
method	LEED	PIFB	LEED	PIFB	DFT	MEIS	PIFB
Ref.	31	Present	Present	35	33	34	Present
Δd_{12}	-8.0 ± 2	−58.5	-11.2 ± 0.7	−11.2	−16	-13 ± 3	−11.4
Δd_{23}	5.5 ± 2	8.1	-4.4 ± 1.4	−34.1	+1.5	-8 ± 5	−9.4
Δr_3			10.2 ± 1.4	22.5	+7	$+8\pm3$	14.5
Δd_{34}	-3.7 ± 2	−0.7	-5.2 ± 1.4	−7.8			
Δd_{45}	$+0.7\pm1$	0.07	-1.4 ± 1.4	−0.5			
Δr_5			4.2 ± 2.1	0.5			

$c(2\times2)$ layer of the substrate. Substrate atoms were placed in their bulk positions in all layers. The numerical values of the forces on the layers have been arbitrarily multiplied by 2.865 for each system to produce displacements in Å, leading to the values given in the columns headed PIFB in Table II. It can be seen that the PIFB calculations reproduce the trends of the experimental results.

C. Surface vibrations

Finally, we note that the enhanced vibrational amplitudes of the surface layers of the clean Al(110) surface are preserved on adsorption (see Table I), as found previously for other alkali/Al adsorption systems.[37] It can also be noted that the vibrational amplitudes of Al atoms in the two sublattices of the rumpled third Al layer differ significantly. The vibrational amplitudes of Al atoms directly beneath Na atoms are enhanced with respect to the remaining Al atoms of this layer.

ACKNOWLEDGMENTS

Support of this work by the Danish Natural Science Research Council is gratefully acknowledged.

[1] A. Schmalz, S. Aminpirooz, L. Becker, J. Haase, J. Neuegebauer, M. Scheffler, D.R. Batchelor, D.L. Adams, and E. Bøgh, Phys. Rev. Lett. **67**, 2163 (1991).
[2] D.L. Adams, Appl. Phys. A: Mater. Sci. Process. **62**, 123 (1996), and references therein.
[3] W. Berndt, D. Weick, C. Stampfl, A.M. Bradshaw, and M. Scheffler, Surf. Sci. **330**, 182 (1995).
[4] M.M. Nielsen, S.V. Christensen, and D.L. Adams, Phys. Rev. B **54**, 17 902 (1996).
[5] J.H. Petersen, A. Mikkelsen, M.M. Nielsen, and D.L. Adams, Phys. Rev. B **60**, 5963 (1999).
[6] B.E. Haydon, K.C. Prince, P.J. Davie, G. Paolucci, and A.M. Bradshaw, Solid State Commun. **4**, 325 (1983).
[7] R.J. Behm, in *Physics and Chemistry of Alkali Metal Adsorption*, edited by H.P. Bonzel, A.M. Bradshaw, and G. Ertl (Elsevier, Amsterdam, 1989), p. 111.
[8] C.J. Barnes, M. Lindroos, D.J. Holmes, and D.A. King, in *Physics and Chemistry of Alkali Metal Adsorption* (Ref. 7), p. 129.
[9] E.C. Sowa, M.A.V. Hove, and D.L. Adams, Surf. Sci. **199**, 174 (1988).
[10] P. Fery, W. Moritz, and D. Wolf, Phys. Rev. B **38**, 7275 (1988).
[11] C.M. Chan, M.A.V. Hove, W.H. Weinberg, and E.D. Williams, Surf. Sci. **91**, 440 (1980).
[12] W. Moritz and D. Wolf, Surf. Sci. **88**, L29 (1979).
[13] K.W. Jacobsen and J.K. Nørskov, Phys. Rev. Lett. **60**, 2496 (1988).
[14] O.B. Christensen and K.W. Jacobsen, Phys. Rev. B **45**, 6893 (1992).
[15] P. Hofmann, S. Bao, K.M. Schindler, O. Schaff, M. Polcik, V. Fritzche, A.M. Bradshaw, R. Davis, and D.P. Woodruff, Surf. Sci. **319**, L7 (1994).
[16] S. V. Hoffmann, Ph. D. thesis, University of Aarhus, 1996.
[17] J. H. Petersen, S. V. Hoffmann, A. Mikkelsen, J. Nerlov, and D. L. Adams (unpublished).
[18] A. Mikkelsen and D.L. Adams, Phys. Rev. B **60**, 2040 (1999).
[19] J.N. Andersen, H.B. Nielsen, L. Petersen, and D.L. Adams, J. Phys. C **17**, 173 (1984).
[20] SAES Getters, Milan, Italy.
[21] D.L. Adams, S.P. Andersen, and J. Burchhardt, in *The Structure of Surfaces III*, edited by S.Y. Tong, M.A.V. Hove, X. Xide, and K. Takayanagi (Springer, Berlin, 1991), p. 156.
[22] D.L. Adams, J. Phys. C **16**, 6101 (1983).
[23] D.L. Adams, V. Jensen, X.F. Sun, and J.H. Vollesen, Phys. Rev. B **38**, 7913 (1988).
[24] J.B. Pendry, *Low Energy Electron Diffraction* (Academic Press, London, 1974).
[25] M.A.V. Hove and S.Y. Tong, *Surface Crystallography by LEED* (Springer-Verlag, Berlin, 1979).

[26] V.L. Moruzzi, J.F. Janak, and A.R. Williams, *Calculated Electronic Properties of Metals* (Pergamon, New York, 1978).

[27] A. Guinier, *X-Ray Diffraction* (Freeman, San Francisco, 1963).

[28] Within the physical model, the accuracy of the intensity calculations depends on the convergence of the lattice sums with respect to the number of lattice points in the calculation of *L*-space scattering matrices; the convergence of the matrix elements of the bulk reflection matrix with respect to the number of doublings in the layer-doubling process; the convergence of the intensities with respect to the number of partial waves and beams used, respectively, in the *L*-space and *k*-space parts of the calculation. Suitable convergence criteria were determined by calculating the root-mean-square (rms) discrepancies between sets of intensity spectra calculated for different criteria. In these calculations, mean-square errors were calculated for the spectra of the individual beams and combined to give an overall mean-square error by weighting the beams according to their energy ranges. For example, with all other criteria set to produce rms errors of less than 0.02 %, the intensity calculations were converged to 0.02 % when using 22 phase shifts for Na, whereas convergence levels of 6 %, 2 %, and 0.2 % were found for 10, 14, and 18 phase shifts, respectively. Similar results were found for Al.

[29] J. Burchhardt, M.M. Nielsen, D.L. Adams, E. Lundgren, and J.N. Andersen, Phys. Rev. B **50**, 4718 (1994).

[30] M.M. Nielsen, J. Burchhardt, and D.L. Adams, Phys. Rev. B **50**, 7851 (1994).

[31] A. Mikkelsen, J. Jiruse, and D.L. Adams, Phys. Rev. B **60**, 7796 (1999).

[32] R. Stumpf and M. Scheffler, Phys. Rev. B **53**, 4958 (1996).

[33] K.M. Ho, C.T. Chan, and K.P. Bohnen, Phys. Rev. B **40**, 9978 (1989).

[34] P. Häberle and T. Gustafsson, Phys. Rev. B **40**, 8218 (1989).

[35] A. Mikkelsen and D.L. Adams (unpublished).

[36] D.P. Woodruff, *The Chemical Physics of Solid Surfaces*, edited by D.A. King and D.P. Woodruff (Elsevier, Amsterdam, 1994), Vol. 7, Chap. 12, p. 465.

[37] M.M. Nielsen, J. Burchhardt, D.L. Adams, E. Lundgren, and J.N. Andersen, Phys. Rev. Lett. **72**, 3370 (1994).